








Interaction-enhanced nesting in spin-fermion and Fermi-Hubbard models

R. Rossi ^{1,2} F. Šimkovic IV ^{3,4,*} M. Ferrero ^{3,4} A. Georges ^{5,4,3,6} A. M. Tsvelik ⁷
N. V. Prokof'ev ⁸ and I. S. Tupitsyn ^{8,†}

¹*Sorbonne Université, CNRS, Laboratoire de Physique Théorique de la Matière Condensée, LPTMC, F-75005 Paris, France*

²*École Polytechnique Fédérale de Lausanne (EPFL), Institute of Physics, CH-1015 Lausanne, Switzerland*

³*CPHT, CNRS, Ecole Polytechnique, IP Paris, F-91128 Palaiseau, France*

⁴*College de France, 11 place Marcelin Berthelot, 75005 Paris, France*

⁵*Center for Computational Quantum Physics, Flatiron Institute, 162 Fifth Avenue, New York, New York 10010, USA*

⁶*DQMP, Université de Genève, 24 quai Ernest Ansermet, CH-1211 Genève, Switzerland*

⁷*Condensed Matter Physics and Materials Science Division, Brookhaven National Laboratory, Upton, New York 11973-5000, USA*

⁸*Department of Physics, University of Massachusetts, Amherst, Massachusetts 01003, USA*



(Received 14 June 2024; accepted 28 August 2024; published 10 September 2024)

The spin-fermion (SF) model postulates that the dominant coupling between low-energy fermions in near critical metals is mediated by collective spin fluctuations (paramagnons) peaked at the Néel wave vector, \mathbf{Q}_N , connecting hot spots on opposite sides of the Fermi surface. It has been argued that strong correlations at hot spots lead to a Fermi surface deformation (FSD) featuring flat regions and increased nesting. This conjecture was confirmed in the perturbative self-consistent calculations when the paramagnon propagator dependence on momentum deviation from \mathbf{Q}_N is given by $\chi^{-1} \propto |\Delta q|$. Using diagrammatic Monte Carlo (diagMC) technique we show that such a dependence holds only at temperatures orders of magnitude smaller than any other energy scale in the problem, indicating that a different mechanism may be at play. Instead, we find that a $\chi^{-1} \propto |\Delta q|^2$ dependence yields a robust finite- T scenario for achieving FSD. To link phenomenological and microscopic descriptions, we applied the connected determinant diagMC method to the $(t - t')$ Hubbard model and found that at large $U/t > 5.5$ before the formation of electron and hole pockets (i) the FSD defined as a maximum of the spectral function is not very pronounced; instead, it is the lines of zeros of the renormalized dispersion relation that deforms toward nesting, and (ii) the static spin susceptibility is well described by $\chi^{-1} \propto |\Delta q|^2$. Flat FS regions yield a nontrivial scenario for realizing a non-Fermi liquid state.

DOI: [10.1103/PhysRevResearch.6.L032058](https://doi.org/10.1103/PhysRevResearch.6.L032058)

Introduction. The two-dimensional spin-fermion model was formulated as an effective theory for near critical metals and used to explain the non-Fermi liquid physics and superconducting instability in doped cuprates [1,2]. In this semiphenomenological model, the low-energy quasiparticles interact with collective magnetic fluctuations, or paramagnons. In some theories of high- T_c superconductors the paramagnons play a role similar to phonons in ordinary metals, with the general concept formulated in Refs. [3,4]. The model has found a wide range of applications in cuprates and iron-based superconductors including proposals for pairing mechanisms in the “strange metal” [5].

On approach to the antiferromagnetic instability, the spectrum of paramagnons softens and strong near-critical

fluctuations may cause the Fermi surface (FS) to change its shape near the hot spots—the FS points connected by the Néel wave vector \mathbf{Q}_N . In what follows we consider the case with eight hot spots when $\mathbf{Q}_N = (\pm\pi, \pm\pi)/a$ with $a = 1$ being the lattice constant. The exchange interaction mediated by the soft modes changes the dispersion relation and, thus, deforms the FS in the vicinity of hot spots, making it flatter and closer to the nesting condition between the opposite FS patches (for the illustration see Fig. 1 in [6]). This remarkable Fermi surface deformation (FSD) originates solely from the strong correlations within the hot spots. However, when it comes to establishing the quantitative description of the phenomenon, one finds that the result crucially depends on the wave vector dependence of the paramagnon propagator χ (its frequency dependence is dominated by Landau damping, $\propto |\omega|$, describing decay of spin waves into particle-hole excitations [2,7]).

The critical Ornstein-Zernike form, $\chi^{-1} \propto |\Delta \mathbf{q}|^2$, with $\Delta \mathbf{q} = \mathbf{q} - \mathbf{Q}_N$, leads to the non-Fermi liquid behavior [1,2,7–11]; the tendency to FSD was established in one-loop RG [1,2]. (A model with four hot spots, when the FS touches the antiferromagnetic Brillouin zone boundary (AFBZB) is a “nonconventional” Fermi liquid state; its self-energy differs from the standard Fermi liquid expectations but the low-energy quasiparticles remain well defined [12,13]). It was

*Present Address: IQM GERMANY GmbH, 80636 München, Germany.

†Contact author: itupitsyn@physics.umass.edu

Published by the American Physical Society under the terms of the [Creative Commons Attribution 4.0 International](https://creativecommons.org/licenses/by/4.0/) license. Further distribution of this work must maintain attribution to the author(s) and the published article's title, journal citation, and DOI.

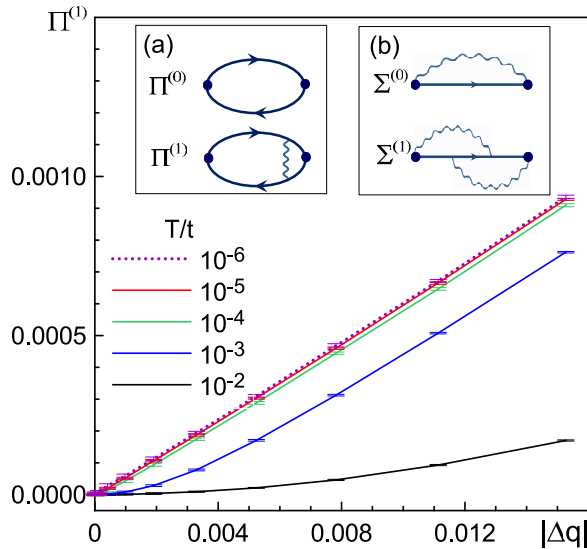


FIG. 1. Polarization $\Pi^{(1)}$ as a function of $|\Delta\mathbf{q}|$ (see text) along the (π, π) direction at zero Matsubara frequency. Insets show leading-order diagrams contributing to (a) polarization function and (b) proper self-energy. All data were obtained for $t'/t = -0.1$, $c = 1$, $g = 1$, and $\eta = 10^{-6}$ at half-filling; in this case the initial angle θ_N is less than 10° .

suggested in Ref. [14] that in the limit of weak coupling and small angle between the \mathbf{Q}_N and FS normal at hot spots, the effective paramagnon propagator takes the form $\chi^{-1} \sim |\Delta q|$. In this case, the outcome of the second-order self-consistent solution is a flow toward flat hot spot domains. However, an attempt of Ref. [15] to verify predictions of Ref. [14] using determinant Monte Carlo simulations [9,16] at temperature $T/E_F \geq 0.005$ did not find evidence for linear momentum dependence $\chi^{-1} \sim |\Delta q|$ despite observing deviations from the Ornstein-Zernike ansatz. A more recent hybrid Monte Carlo simulation for larger system sizes have reached similar conclusions [17].

It should be noted that since interactions mediated by critical modes do not displace quasiparticles along the FS, well nested flat regions effectively act as one-dimensional subsystems [6]. This is an alternative scenario for realizing the non-Fermi liquid state that explains several important properties of the pseudogap regime in cuprates, including the excitation spectrum and transport phenomena (see, for instance, [18,19]).

In this Letter, we address the FSD problem within the spin-fermion and $(t - t')$ Hubbard models. Using diagrammatic Monte Carlo (diagMC) method we first verify the self-consistent scenario of Ref. [14] for the SF model and demonstrate that it holds only at ultralow temperatures. Next, to connect phenomenological considerations with microscopic physics, we apply the connected determinant diagMC technique (CDet) to the $(t - t')$ Hubbard model to reveal how FSD develops in this case and what is the corresponding momentum dependence of the spin susceptibility.

The diagMC approach combines advantages of quantum field-theory tools with power of MC sampling of complex configuration spaces [20,21]. It works directly in the thermodynamic limit and does not suffer from the conventional

fermionic sign problem [22], making it suitable for solving systems with arbitrary dispersion relations and shapes of the interaction potential [23–25]. The CDet approach [26] performs efficient summation of all diagram topologies “on the fly” and currently represents one of the most advanced unbiased techniques for the Hubbard model.

Models. In the SF model with hot spots, Landau damping renders the “bare” quadratic dependence of χ on frequency, irrelevant at low temperature. This allows one to formulate the model in the Hamiltonian form [1,2]:

$$H = \sum_{\mathbf{k}, \alpha} \epsilon_{\mathbf{k}} c_{\mathbf{k}, \alpha}^\dagger c_{\mathbf{k}, \alpha} + \sum_q \chi_0^{-1}(q) \mathbf{S}_q \cdot \mathbf{S}_{-q} + g \sum_{\mathbf{k}, \mathbf{q}, \alpha, \beta, i} c_{\mathbf{k}+\mathbf{q}, \alpha}^\dagger \sigma_{\alpha, \beta}^i c_{\mathbf{k}, \beta} S_{-q}^i, \quad (1)$$

where $c_{\mathbf{k}, \alpha}^\dagger$ is the fermion creation operator in the state with momentum \mathbf{k} and spin projection α , σ^i are Pauli matrices ($i = x, y, z$), g is the SF coupling constant, $\epsilon_{\mathbf{k}}$ is the bare electron dispersion, and \mathbf{S} is the collective spin degree of freedom. In what follows we choose $\epsilon_{\mathbf{k}}$ as the tight-binding dispersion relation on the square lattice with two hopping amplitudes, t and t' ($t = 1$ in our units), yielding $\epsilon_{\mathbf{k}} = -2t(\cos k_x + \cos k_y) - 4t' \cos k_x \cos k_y$.

Feynman diagrams for proper self-energy, $\Sigma(\mathbf{q}, \omega_n)$, and polarization, $\Pi(\mathbf{q}, \omega_m)$, where ω_n and ω_m are fermionic and bosonic Matsubara frequencies, respectively, follow from the standard rules for the conventional and the skeleton representations, and have the same structure as for fermions interacting via

$$V_{i,j}(\mathbf{q}, \omega_m) = -\frac{g}{4} \frac{(\sigma_i \sigma_j)}{\gamma |\omega_m| + \chi_0^{-1}(|\mathbf{q} - \mathbf{Q}_N|)}, \quad (2)$$

where σ^a are Pauli matrices acting on the quasiparticle’s spins and γ is the Landau damping constant (in what follows we take $\gamma/t = 1$). This form respects the spin $SU(2)$ symmetry [on the square lattice all four vectors $(\pm\pi, \pm\pi)$ are formally identical to \mathbf{Q}_N].

The standard Fermi-Hubbard model on a square lattice at half filling is parametrized by the nearest- and next-nearest-neighbor hopping amplitudes t and t' and on-site repulsion U (see, for instance, Ref. [27]). For a description of the corresponding diagrammatic series and their treatment see Refs. [26–28].

SF model. We start by verifying the scenario put forward in Ref. [14], which corresponds to the limit of weak coupling and small angle θ_N between \mathbf{Q}_N and the FS normal at the hot spot. Building on the one-loop RG result of Ref. [8] that dynamical exponent z decreases from $z = 2$, it was conjectured that the flow is toward $\chi^{-1} = [c(|\Delta\mathbf{q}_x| + |\Delta\mathbf{q}_y|) + |\omega|]$. Moreover, it was shown that χ^{-1} reproduces itself within the Dyson-Schwinger equation at the level of two skeleton diagrams for the polarization Π , and, thus, represents the proper effective paramagnon propagator. The linear in momentum term is generated by the second-order diagram, see $\Pi^{(1)}$ in Fig. 1(a), while higher-order diagrams were argued to be small. This form of χ then leads to the FSD with flat hot spots because, for renormalized spectrum, θ_N tends to zero. The major drawback of this scenario is the assumption that

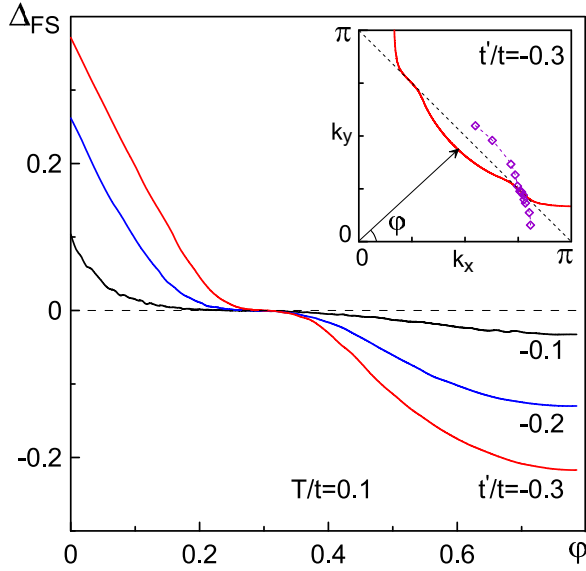


FIG. 2. Deviation of the FS from the AFBZB (dashed line) in momentum space as a function of angle φ for the SF model. The inset displays one segment of the FS (solid red line) extracted from $E_{\mathbf{k}} = 0$ (see text). The dashed diamond curve shows part of the DLS corresponding to the maxima of $|\text{Im}\Sigma_{\mathbf{k}}^{(0)}|$. All results are obtained for $T/t = 0.1$, $c = 1$, $g/t = 0.4$, and $\eta = 10^{-3}$.

the renormalized coupling constant is small, for which there is no evidence.

Using the diagMC technique for Eqs. (1) and (2) with $\chi_0^{-1} = c(|\Delta\mathbf{q}_x| + |\Delta\mathbf{q}_y|) + \eta$, where $\eta \sim \xi^{-1}$ is the inverse correlation length, we computed the polarization and the proper self-energy diagrams shown in both insets of Fig. 1, and confirmed the prediction of Ref. [14] regarding the formation of flat regions around the hot spots in the limit of interest. However, the entire scheme turned out to be extremely fragile against finite temperature effects.

Figure 1 shows that already at $10^{-4} < T/t < 10^{-3}$ the momentum dependence of $\Pi^{(1)}$ deviates from the linear one. On the one hand this may explain why Ref. [15] did not observe it. On the other hand, our results invalidate the FSD scenario proposed in Ref. [14] for $T/t > 10^{-4}$. This ultralow temperature scale finds no explanation in any of the microscopic system parameters or the effective theory of Ref. [14]. Thus, if FSD is observed in a microscopic model at higher temperature, it has to be a different effective theory.

If we proceed with computing the self-energy $\Sigma^{(0)}$ [see Fig. 1(b)] with $\chi_0^{-1} = c^2\Delta\mathbf{q}^2 + \eta^2$ and use it to determine the renormalized dispersion relation, $E_{\mathbf{k}} = \epsilon_{\mathbf{k}} + \text{Re}\Sigma_{\mathbf{k}}^{(0)}(i\omega \rightarrow 0) - \mu$, counted from the chemical potential μ , we obtain results for the FSD shown in Fig. 2. We plot the distance Δ_{FS} between the FS and AFBZB as a function of angle $\varphi = \tan^{-1}[(k_y - \pi)/(k_x - \pi)]$ with $\Delta_{FS} = 0$ corresponding to the hot spot. Clearly, it is possible to produce flat hot-spot regions with quadratic momentum dependence of χ at temperatures orders of magnitude higher than the limit established above for the linear momentum ansatz, including the $t'/t = -0.3$ case when the initial angle θ_N is relatively large.

When $\text{Re}\Sigma_{\mathbf{k}}$ and $\text{Im}\Sigma_{\mathbf{k}}$ have similar magnitudes, zeros of $E_{\mathbf{k}}$ may not coincide with spectral intensity peaks measured by ARPES. In this case, one may consider defining FS and

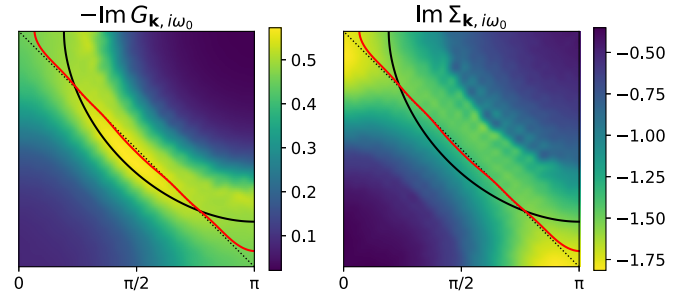


FIG. 3. Momentum-resolved spectral function proxy (left) and imaginary part of the self-energy (right) at the lowest Matsubara frequency of the half-filled two-dimensional Hubbard model with parameters $U/t = 5.75$, $t'/t = -0.3$, and $T/t = 1/7$. The calculation was performed on a 60×60 lattice up to ninth order in the interaction strength, and, for visualization purposes, it was assumed that the self-energy is zero outside a 60×60 box around the origin. We plot here a quarter of the Brillouin zone. The black line is the noninteracting FS, while the red line is the solution of $E_{\mathbf{k}} = 0$ (with full $\Sigma_{\mathbf{k}}$).

the so-called Dzyaloshinskii-Luttinger surface (DLS) [29,30] from the maxima and minima of spectral intensity, respectively. The purple diamond curve in the inset of Fig. 2 shows part of DLS extracted from the maxima of $|\text{Im}\Sigma_{\mathbf{k}}^{(0)}|$ at the smallest Matsubara frequency, which also features a flat hot spot. Within hot spots $|\text{Im}\Sigma_{\mathbf{k}}|$ is large, leading to suppressed intensity in the nested regions.

It was suggested in Ref. [6] that $\chi^{-1} \propto |\Delta\mathbf{q}|^2$ within the SF model confines quasiparticles within the flat FS regions, and, as a result, these parts of FS form a one dimensional subsystem weakly coupled to the rest of the FS. At sufficiently low temperature, the state should be viewed as mixture of the non-Fermi liquid whose physics is dominated by strong one-dimensional fluctuations and the conventional Fermi liquid. Eventually, the flat regions are gapped out leaving behind a state with reduced FS [18,19].

Since the perturbative expansion for $\chi_0^{-1} = c^2\Delta\mathbf{q}^2 + \eta^2$ with vanishing η breaks down, one has to assume that all vertex corrections are ultimately reduced to the renormalization of constants in the effective theory. The best way to verify this assumption and to establish a link between the microscopic physics and phenomenological treatments is to perform CDet simulations of the two-dimensional $(t - t')$ Hubbard model at half filling.

Fermi-Hubbard model. The Fermi-Hubbard model on the square lattice is the most studied prototypical model in the context of cuprate superconductors. Nevertheless, the possibility of the FSD toward flat hot spots in this model was never addressed by unbiased first-principles methods. Our approach is to employ the CDet technique at fixed density [27,31] to evaluate Feynman diagrams up to high order to accurately compute the shape of the Fermi surface and spin susceptibility for the $(t - t')$ Hubbard model at half-filling (for the series resummation procedure, see the Supplemental Material [32]). The choice of half-filling was dictated by our goal of maximizing antiferromagnetic correlations and avoiding competing ordering tendencies.

We display in Fig. 3 our results for a representative point $U/t = 5.75$ and $T/t = 1/7$. Defining the FS as the maximum

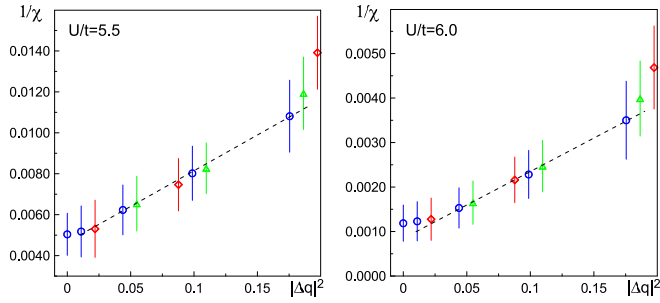


FIG. 4. Inverse static spin susceptibility as a function of $|\Delta\mathbf{q}|^2 \equiv |\mathbf{q} - \mathbf{Q}_N|^2$ for the $(t - t')$ Fermi-Hubbard model at half-filling and $U/t = 5.5, 6.0$, $T/t = 0.1$, $t'/t = -0.3$. Plots are presented for (red diamonds) $(0, 0) \rightarrow (\pi, \pi)$ direction; (blue circles) $(0, \pi) \rightarrow (\pi, \pi)$ direction; and (green triangles) an arbitrary direction to (π, π) . Dashed line is the fit demonstrating $a|\Delta q|^2 + b$ behavior of χ^{-1} at small deviations $|\Delta q|$ with momentum independent a and b .

of the spectral function proxy at the smallest Matsubara frequency, $-ImG_{\mathbf{k}, i\omega_0}$, we see that it does not deform much. It is instead the line of zeros of $E_{\mathbf{k}}$ that undergoes significant deformation toward nesting. However, the imaginary part of Σ is large all along the AFBZB, and largest at the “antinode” $\mathbf{k} = (\pi, 0)$ and the symmetry related points, as is clear from the second panel of Fig. 3. It suppresses the spectral weight along the AFBZB, indicating that the potential excitations suggested by the renormalized quasiparticle dispersion (which neglects $Im\Sigma$) are in fact destroyed by large scattering with momentum transfer close to \mathbf{Q}_N . We emphasize that this is in strong contrast to what is expected from a weak-coupling antiferromagnetic spin-fluctuation theory, where one would expect that the maximum of the imaginary part of the self-energy would lie on a (π, π) -shifted version of FS. Hence, this nesting property of the self-energy is a strong-coupling non-perturbative effect. Correspondingly, it is close to the antinode that the real part of the self-energy has the strongest renormalization effect on the dispersion relation (see also the Supplemental Material [32]). We finally note that the effective field theory of Ref. [14] is not applicable at considered temperatures.

The momentum dependence of the spin susceptibility is presented in Fig. 4. For small $|\Delta q|$ the response is nearly isotropic and closely follows the $c^2|\Delta q|^2 + \xi^{-2}$ behavior with both c and ξ strongly dependent on U . At $U/t = 6.5$ the correlation length is already about five lattice spacing. We take these results as direct confirmation that diverging spin correlations with quadratic dependence on Δq are responsible for the formation of flat hot regions along AFBZB, in the $(t - t')$ Fermi-Hubbard model. Once such regions form, they effectively act as one-dimensional systems with non-Fermi liquid properties.

Discussion and conclusion. Using diagrammatic Monte Carlo methods, we have considered different mechanisms and effective theories for formation of flat hot spots that amplify the nesting conditions in metals with near-critical antiferromagnetic correlations. For the SF model, we confirmed predictions of the weak-coupling theory with linear in momentum dependence of the inverse paramagnon propagator χ^{-1} . However, this linear dependence holds only at unreasonably low temperature. The quadratic momentum dependence of χ^{-1} is robust against finite-temperature effects and also leads to flat Fermi surface domains near the hot spots, but the corresponding effective field theory should assume that higher-order vertex corrections are already accounted for in the form of $\chi^{(0)}$.

High-order connected determinant Monte Carlo simulations of the $(t - t')$ Fermi-Hubbard model at half-filling reveal that the Fermi surface based on spectral intensity maxima does not undergo dramatic deformation toward flat AFBZB. It is instead the lines of zero of the renormalized quasiparticle dispersion that deforms toward nesting. This can be explained by a nesting property of the self-energy, which becomes large along the AFBZB, a typical strong coupling effect. In the same parameter regime, χ has a sharp peak at the Néel wave vector $\mathbf{Q}_N = (\pm\pi, \pm\pi)$, and the best description of the dependence of χ^{-1} on momentum for small deviations from \mathbf{Q}_N is quadratic.

The key common aspect between the SF and Hubbard model is that the quasiparticle dispersion is renormalized toward nesting. In the Hubbard model this, in turn, leads to enhanced scattering along the AFBZB which destroys quasiparticle coherence in this “hot” region; this effect being stronger near the antinodes (presumably due to the proximity of the van Hove singularity). In the spin-fermion model, spectral intensity also gets suppressed within flat hot spots.

At zero temperature, we expect from, e.g., mean-field theory that the half-filled $(t - t')$ Hubbard model at intermediate values of U has a metallic ground state with a FS reconstructed into hole and electron pockets due to antiferromagnetic ordering (at larger U , it becomes a Mott insulator with a fully gapped FS). Our results show that further understanding of how this state is reached as temperature is lowered and the correlation length grows, and of the corresponding fermiology at low but finite temperature, should take into account the quasi-one-dimensional nature of nested hot regions, as was suggested in [6].

Acknowledgments. Authors are grateful to A. Chubukov and P. Lunts for helpful discussions. I.S.T. and N.V.P. acknowledge support from the U.S. Department of Energy, Office of Science, Basic Energy Sciences, under Award No. DE-SC0023141. A.M.T. was supported by Office of Basic Energy Sciences, Material Sciences and Engineering Division, U.S. Department of Energy (DOE) under Contract No. DE-SC0012704. The Flatiron Institute is a division of the Simons Foundation.

[1] Ar. Abanov and A. V. Chubukov, Spin-Fermion model near the quantum critical point: One-loop renormalization group results, *Phys. Rev. Lett.* **84**, 5608 (2000).

[2] Ar. Abanov, A. V. Chubukov, and J. Schmalian, Quantum-critical theory of the spin-fermion model and its application to cuprates: Normal state analysis, *Adv. Phys.* **52**, 119 (2003).

- [3] J. A. Hertz, Quantum critical phenomena, *Phys. Rev. B* **14**, 1165 (1976).
- [4] A. J. Millis, Effect of a nonzero temperature on quantum critical points in itinerant fermion systems, *Phys. Rev. B* **48**, 7183 (1993).
- [5] X. Wang, Y. Schattner, E. Berg, and R. M. Fernandes, Superconductivity mediated by quantum critical antiferromagnetic fluctuations: The rise and fall of hot spots, *Phys. Rev. B* **95**, 174520 (2017).
- [6] A. M. Tsvelik, Ladder physics in the spin fermion model, *Phys. Rev. B* **95**, 201112(R) (2017).
- [7] B. L. Altshuler, I. B. Ioffe and A. J. Millis, Low-energy properties of fermions with singular interactions, *Phys. Rev. B* **50**, 14048 (1994).
- [8] M. A. Metlitski and S. Sachdev, Quantum phase transitions of metals in two spatial dimensions. II. Spin density wave order, *Phys. Rev. B* **82**, 075128 (2010).
- [9] E. Berg, M. A. Metlitski, and S. Sachdev, Sign problem free quantum Monte Carlo of the onset of antiferromagnetism in metals, *Science* **338**, 1606 (2012).
- [10] S. A. Maier and P. Strack, Universality in antiferromagnetic strange metals, *Phys. Rev. B* **93**, 165114 (2016).
- [11] M. H. Gerlach, Y. Schattner, E. Berg, and S. Trebst, Quantum critical properties of a metallic spin-density-wave transition, *Phys. Rev. B* **95**, 035124 (2017).
- [12] D. Bergeron, D. Chowdhury, M. Punk, S. Sachdev, and A.-M. S. Tremblay, Breakdown of Fermi liquid behavior at the $(\pi, \pi) = 2k_F$ spin-density wave quantum-critical point: The case of electron-doped cuprates, *Phys. Rev. B* **86**, 155123 (2012).
- [13] Y. Wang and A. Chubukov, Quantum-critical pairing in electron-doped cuprates, *Phys. Rev. B* **88**, 024516 (2013).
- [14] A. Schliefl, P. Lunts, and S.-S. Lee, Exact critical exponents for the antiferromagnetic quantum critical metal in two dimensions, *Phys. Rev. X* **7**, 021010 (2017).
- [15] C. Bauer, Y. Schattner, S. Trebst, and E. Berg, Hierarchy of energy scales in an O(3) symmetric antiferromagnetic quantum critical metal: A Monte Carlo study, *Phys. Rev. Res.* **2**, 023008 (2020).
- [16] R. Blankenbecler, D. J. Scalapino, and R. L. Sugar, Monte Carlo calculations of coupled boson-fermion systems. I, *Phys. Rev. D* **24**, 2278 (1981).
- [17] P. Lunts, M. S. Albergo, and M. Lindsey, Non-hertz-millis scaling of the antiferromagnetic quantum critical metal via scalable hybrid Monte Carlo, *Nat. Commun.* **14**, 2547 (2023).
- [18] T. M. Rice, N. J. Robinson, and A. M. Tsvelik, Umklapp scattering as the origin of T -linear resistivity in the normal state of high- T_c cuprate superconductors, *Phys. Rev. B* **96**, 220502(R) (2017).
- [19] L. Classen, N. J. Robinson, and A. M. Tsvelik, Ladderlike optical conductivity in the spin-fermion model, *Phys. Rev. B* **99**, 115110 (2019).
- [20] E. Kozik, K. Van Houcke, E. Gull, L. Pollet, N. Prokof'ev, B. Svistunov, and M. Troyer, Diagrammatic Monte Carlo for correlated fermions, *Europhys. Lett.* **90**, 10004 (2010).
- [21] K. Van Houcke, F. Werner, E. Kozik, N. Prokof'ev, B. Svistunov, M. J. H. Ku, A. T. Sommer, L. W. Cheuk, and A. Schirotzek, Feynman diagrams versus Fermi-gas Feynman emulator, *Nat. Phys.* **8**, 366 (2012).
- [22] R. Rossi, N. Prokof'ev, B. Svistunov, K. Van Houcke, and F. Werner, Polynomial complexity despite the fermionic sign, *Europhys. Lett.* **118**, 10004 (2017).
- [23] I. S. Tupitsyn, A. S. Mishchenko, N. Nagaosa, and N. Prokof'ev, Coulomb and electron-phonon interactions in metals, *Phys. Rev. B* **94**, 155145 (2016).
- [24] I. S. Tupitsyn and N. V. Prokof'ev, Stability of Dirac liquids with strong Coulomb interaction, *Phys. Rev. Lett.* **118**, 026403 (2017).
- [25] J. P. F. Le Blanc, K. Chen, K. Haule, N. V. Prokof'ev, and I. S. Tupitsyn, Dynamic response of an electron gas: Towards the exact exchange-correlation kernel, *Phys. Rev. Lett.* **129**, 246401 (2022).
- [26] R. Rossi, Determinant diagrammatic Monte Carlo algorithm in the thermodynamic limit, *Phys. Rev. Lett.* **119**, 045701 (2017).
- [27] F. Šimkovic IV, R. Rossi, and M. Ferrero, Two-dimensional Hubbard model at finite temperature: Weak, strong, and long correlation regimes, *Phys. Rev. Res.* **4**, 043201 (2022).
- [28] A. Wietek, R. Rossi, F. Šimkovic IV, M. Klett, P. Hansmann, M. Ferrero, E. M. Stoudenmire, T. Schäfer, and A. Georges, Mott insulating states with competing orders in the triangular lattice Hubbard model, *Phys. Rev. X* **11**, 041013 (2021).
- [29] I. Dzyaloshinskii, Some consequences of the Luttinger theorem: The Luttinger surfaces in non-Fermi liquids and Mott insulators, *Phys. Rev. B* **68**, 085113 (2003).
- [30] M. Fabrizio, Emergent quasiparticles at Luttinger surfaces, *Nat. Commun.* **13**, 1561 (2022).
- [31] F. Šimkovic, R. Rossi, A. Georges, and M. Ferrero, Origin and fate of the pseudogap in the doped Hubbard model, [arXiv:2209.09237](https://arxiv.org/abs/2209.09237).
- [32] See Supplemental Material at <http://link.aps.org/supplemental/10.1103/PhysRevResearch.6.L032058> for more details on the resummation technique, spectral function, and dispersion renormalization of the Hubbard model.